ADVANCES IN GEODESY AND GEOINFORMATION
(formerly GEODESY AND CARTOGRAPHY)
Vol. 74, no. 2, article no. e71, 2025

© Polish Academy of Sciences
https://doi.org/10.24425/agg.2025.154155

Original paper

Multi-temporal analysis and forecasting of shoreline dynamics along the Badagry coastline, Nigeria, using integrated remote sensing and statistical approaches

Ekundayo Adesina[1]*, Oluibukun Ajayi[1,2], Joseph Odumosu[2], Kate Akpur[1]

[1]Federal University of Technology, Minna, Nigeria
e-mail: adegeoworldsolutions@gmail.com; ORCID: http://orcid.org/0000-0001-9526-4540
e-mail: oajayi@nust.na; ORCID: http://orcid.org/0000-0002-9467-3569
e-mail: kateakpur@gmail.com; ORCID: http://orcid.org/0009-0001-5780-0856

[2]Namibia University of Science and Technology, Windhoek, Namibia
e-mail: odumossu4life@yahoo.com; ORCID: http://orcid.org/0000-0003-1604-4924

*Corresponding author: Kate Akpur, e-mail: adegeoworldsolutions@gmail.com

Received: 2024-06-14 / Accepted: 2025-09-11

Abstract: Coastal areas are essential for human welfare but are increasingly vulnerable to environmental and anthropogenic pressures. Accurate shoreline monitoring is for sustainable coastal management. This study undertakes a multi-temporal analysis of the Badagry coastline, Nigeria, from 1982 to 2022, using Landsat (MSS, TM, ETM+), Landsat 8 OLI, and Sentinel-2A imagery. Shoreline change rates using the Digital Shoreline Analysis System (DSAS) with End Point Rate, Linear Regression Rate, and Weighted Linear Regression models. The analysis reveals a complex dynamic where a net accretionary trend masks a critical hotspot of severe erosion. This erosional pattern is in the central and western portions of the study area, particularly downdrift of the Badagry Creek inlet. The Linear Regression Rate model demonstrated a strong statistical fit to the historical data, with R^2 values consistently exceeding 0.9. The LRR indicated a maximum accretion rate of +5.32 m/yr. However, the End Point Rate model captured severe localized erosion, with rates reaching up to –0.65 m/yr in specific hotspots. These findings provide a classic example of an interrupted littoral system, a phenomenon observed globally where coastal engineering structures disrupt natural sediment transport. The results strongly suggest that while natural depositional processes, driven by the regional longshore sediment transport system, are active, localized anthropogenic activities, maintenance, and jetty construction at the Badagry Creek inlet are the primary drivers of significant downdrift erosion. The study emphasizes the need to shift from uniform coastal protection policies to spatially targeted management interventions targeting erosion hotspots to prevent further degradation.

Keywords: Badagry coastal shoreline changes, DSAS, interrupted littoral drift, end point rate, linear regression rate

The Author(s). 2025 Open Access. This article is distributed under the terms of the Creative Commons Attribution 4.0 International License (http://creativecommons.org/licenses/by/4.0/), which permits unrestricted use, distribution, and reproduction in any medium, provided you give appropriate credit to the original author(s) and the source, provide a link to the Creative Commons license, and indicate if changes were made.

1. Introduction

The unprecedented rise in sea levels is causing significant changes along coastlines worldwide. This phenomenon results in more extensive beach erosion, land submersion, and coastal inundation (IPCC, 2023). These changes severely endanger ecosystems, infrastructure, and human settlements (Nicholls et al., 2011; Giardino et al., 2018; Young and Carilli, 2018; Vousdoukas et al., 2020; Adesina et al., 2022) predicted that by 2050, rising sea levels and more intense storms could force nearly 200 million people to relocate. The situation poses significant risks for coastal ecosystems and communities, especially those dependent on fishing in low-lying regions. Areas with low elevation and limited sediment availability are more vulnerable to shoreline retreat and coastal erosion. It highlights the urgent need for attention and action (IPCC, 2023).

Detecting and mapping the coastline is one of the most crucial techniques for assessing coastal erosion and accretion and studying the dynamics of coastal morphology (Adeaga et al., 2021; Daniela et al., 2018). Because of its high precision, increased efficiency, and cost-effectiveness, remote sensing is a more effective means to monitor shoreline change in coastal areas than traditional survey methods (Thakur et al., 2017; Arjasakusuma et al., 2021), especially in real-time. An essential component of coasts is the shoreline, a linear structure on Earth's surface that constantly changes in form and location (Roy et al., 2018; Natesan, et al., 2013). Both natural and artificial forces influence shoreline alterations. The shoreline is a variety of natural elements, including geology, geomorphology, storm surges, wind speed, tidal currents, and wave height, which are all exacerbated by sea level rise and yearly variations in precipitation (Shetty et al., 2015; Boateng et al., 2016; Hakkou et al., 2018; Tiemele et al., 2022; IPCC, 2023).

Moreover, human modifications to coastal systems, such as urbanization, harbor defense engineering structures, buildings, sand, vegetation clearance, dam development, etc., also contribute to changes in the coastal environment (Obowu and Abam, 2014). These alterations frequently result in silt buildup or erosion, flooding, and other problems for coastal areas (Aman et al., 2019). Human activities, whether direct or indirect, impact the geomorphology and processes of the shore (Brown et al., 2017). Coastal erosion is a significant marine geologic challenge that poses different levels of risk depending on its sources (Mentaschi et al., 2018; Pollard et al., 2015). The urgent need for adaptation is highlighted by increasing coastal hazards and nearby development. Implementing adaptation strategies is hindered by various technological, financial, economic, and social challenges (Neide et al., 2022). According to Cooper et al. (2020), modelling coastal landscapes and maintaining ecosystem services requires shoreline dynamics, which are often characterized by coastal erosion and recurrent floods (Smail et al., 2019). Studying how shorelines change is crucial for managing sustainable coasts and preventing erosion. Because shorelines are constantly shifting, it's essential to use an indicator that accounts for their natural variability over time and space. It is key to understanding coastal evolution (Boak and Turner, 2005).

However, optical imaging satellites recently pinpointed coastline locations (Jawak and Luis, 2014; Duru, 2017; Gumus et al., 2021; Wu et al., 2022). The scientists, engineers, planners, and coastal managers use it as a crucial indicator for comprehending how

coastlines change and evolve (Mobio et al., 2024). Remote sensing data is now widely available and provides an affordable way to access long-term coastal change measurements within the last thirty years at many different sites throughout the world (Donchyts et al., 2016; Luijendijk et al., 2018; Mentaschi et al., 2018; Ajayi et al., 2023; This study investigates the changes caused by tidal flooding and wave impacts on the coastal plain of Badagry seashore in Lagos State, Nigeria, between 1982 and 2022, which may be further intensified by rising sea levels due to global warming (Ogunrayi et al., 2023).

The hazards of accelerated erosion related to coastal modifications have been the subject of numerous scientific investigations. Komolafe et al. (2022) investigated coastal changes using satellite images from 1987 to 2017 in the Ilaje region. Ogunrayi et al. (2023) matched satellite photographs from 1986 and 2013 with a topographic map from 1969 using statistical methods like endpoint rate and net shoreline movement (NSM) during various periods. Komolafe et al. (2022) also examined changes in the coastal environment using the methodologies of linear regression, rate endpoint, and root mean square error (RMSE). Similarly, Oyedepo and Oluyege (2024) investigated variations in coastal positions. While these studies provide valuable regional context, their shorter timeframes and broader spatial scales present a critical limitation. They often fail to capture the multi-decadal persistence of trends or robustly link shoreline dynamics to specific, localized anthropogenic drivers. A significant research gap, therefore, exists in conducting a high-resolution, 40-year analysis focused on the Badagry coastline that integrates early Landsat archives with modern Sentinel-2 imagery. This study addresses this gap by providing the most detailed long-term assessment of this coastal segment to date, beyond general trend analysis to pinpoint erosion hotspots and identify their primary geomorphic and anthropogenic causes.

This study evaluates changes along the Badagry coastline using methods such as the weighted linear regression endpoint and the linear regression rate to calculate coastal change rates. By analyzing multi-temporal satellite images, the research aims to examine shoreline alterations, accretion, and coastal erosion for 40 years. Additionally, the study seeks to project shoreline protection measures for 2035 and assess the rate of change along the Badagry coast. This information will aid decision-makers in determining the suitability of coastal zones for various upcoming development projects.

2. Study area

Badagry Local Government Area (LGA) is located approximately on latitude1 7°15′N to 7°00′N and longitude 5°00′W to 7°00′W. To its east lies Ologe Lagoon, to its north Ogun State, to its south the Atlantic Ocean, and to its west the Republic of Benin. Badagry (traditionally known as Gbagle) is a coastal town and local government area (LGA) in Lagos State, Nigeria. It is between Lagos and the border with Benin at Seme. According to a 2022 population projection, the population of Badagry is around 241,093 people. Badagry Local Government Area covers an area of 498 km^2. Another aspect peculiar to the area is the tourist attraction sites in this region. Figure 1 shows the map of the study area.

The Badagry coastline is part of the transgressive barrier-lagoon complex of the Bight of Benin, characterized by a narrow, sandy beach fronting a series of lagoons and creeks, most notably the Badagry Creek. Geomorphologically, the coast consists of fine to medium-grained quartz sand and high-energy wave conditions from the South Atlantic Ocean. The dominant wave direction is from the southwest, driving a significant east-directed longshore sediment transport system (Ibe, 1988; Anthony et al., 2015). The tidal regime is microtidal, with a mean spring tidal range of approximately 1.2 m. This high-energy, transport-dominated environment makes the coastline inherently dynamic. Anthropogenic pressures are significant, including sand mining, the construction of local jetties, and increasing urbanization near the coast. These factors, combined with the low-lying topography, increase its vulnerability to erosion and flooding.

A critical anthropogenic influence within the study area is the management of the Badagry Creek inlet. This inlet, a key navigation channel for local maritime traffic, has been subject to periodic maintenance dredging to ensure navigability. Historical records and project timelines indicate that the planning and initial construction of modern jetties and breakwaters associated with the Badagry Deep Seaport project began in the early 2010s, with major agreements signed around 2016. Furthermore, significant maintenance dredging campaigns, likely in preparation for this larger development and to maintain existing channels, were reported to have intensified around 2008 and again post-2015. These structures and activities at the inlet directly intercept the natural east-directed longshore sediment transport, creating the conditions for the sediment starvation and downdrift erosion observed in the central portion of the coastline. Figure 1 shows the study area map.

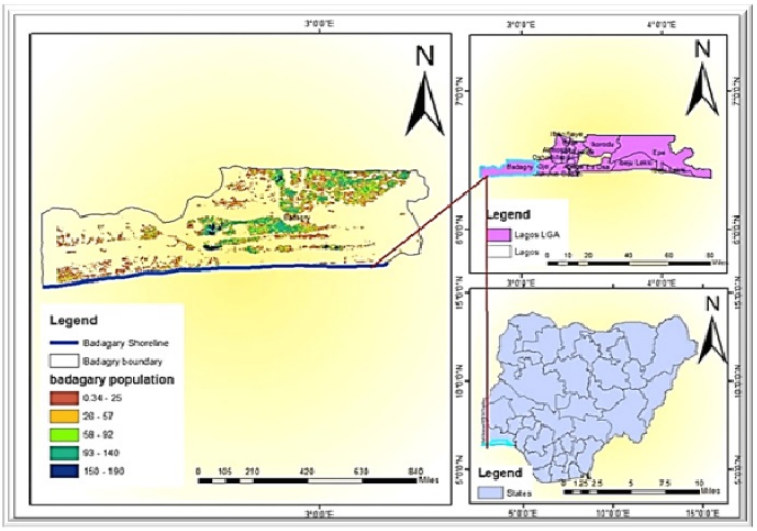

Fig. 1. Study area map

3. Materials and methods

This section outlines the methodology utilized to study shoreline dynamics from 1982 to 2022. The workflow involved three main stages: (1) acquisition and pre-processing of multi-temporal satellite imagery; (2) semi-automated shoreline extraction and associated uncertainty assessment; and (3) calculation of historical change rates and future shoreline projection using the Digital Shoreline Analysis System (DSAS). A detailed methodological flowchart is in Figure 2.

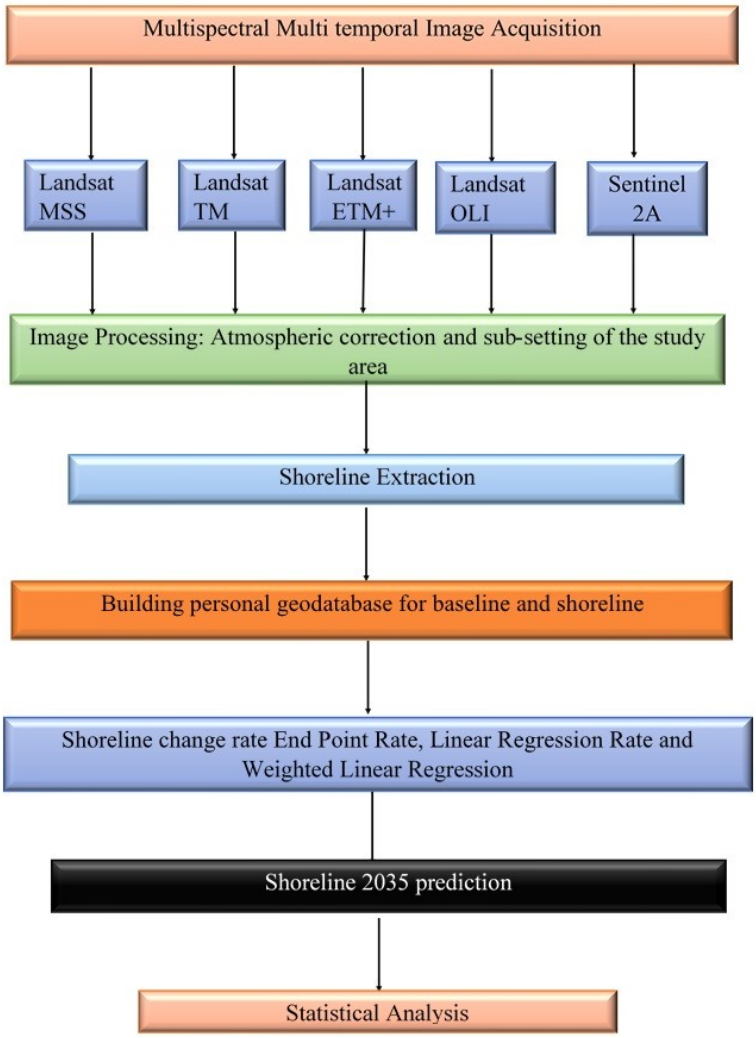

Fig. 2. Methodology flow diagram

3.1. Data acquisition and shoreline extraction

The shorelines and corresponding changes over the last 40 years were retrieved using satellite images and GIS techniques. Between 1982 and 2022, a selection of nine years, specifically 1982, 1987, 1992, 1997, 2002, 2007, 2012, 2017, and 2022, was used for this investigation based on data availability. Table 1 presents the specific attributes of the images used. The alterations in the vector-form shorelines using the Digital Shoreline Analysis System (DSAS) software extension (Thieler et al., 2009), which operates within the ArcGIS environment (ArcGIS Desktop version 10.8).

Table 1. Details of satellite images used in the study

Data	Type	Path/Row	Source	Spatial resolution (m)	Data of acquisition
Landsat MSS	Secondary	189/053	USGS	60	02/05/1982
Landsat MSS	Secondary	189/053	USGS	60	01/02/1987
Landsat TM	Secondary	189/053	USGS	30	02/03/1992
Landsat TM	Secondary	189/053	USGS	30	01/01/1997
Landsat ETM+	Secondary	189/053	USGS	30	02/03/2002
Landsat ETM+	Secondary	189/053	USGS	30	01/01/2007
Landsat ETM+	Secondary	189/053	USGS	30	01/01/2012
Landsat 8 OLI	Secondary	189/053	USGS	30	01/01/2017
Sentinel 2A	Secondary	T31NFJ	Copernicus Archive	10	01/01/2022

*__MSS, TM, ETM+, OLI__: These are acronyms for different sensors aboard the Landsat satellite series: Multi-Spectral Scanner, Thematic Mapper, Enhanced Thematic Mapper Plus, and Operational Land Imager, respectively. They represent different generations of technology with varying spatial resolutions.
Secondary: This indicates that the data was not collected primarily by the authors for this study but from existing, publicly available archives.
USGS: United States Geological Survey, the primary provider of Landsat data.
Copernicus Archive: The data repository for the European Union's Earth Observation Programme manages the Sentinel satellites.

Thus, shorelines were extracted from the multi-temporal satellite imagery using a semi-automated approach based on the Modified Normalized Difference Water Index (*MNDWI*) (Duru, 2017; Gumus et al., 2021), which is effective at separating land and

water boundaries (Xu, 2006). The *MNDWI* was calculated for each image using the Green and Short-Wave Infrared (*SWIR*1) bands presented in Eq. 1 (Xu, 2006):

$$MNDWI = (Green - SWIR1)/(Green + SWIR1). \tag{1}$$

The resulting raster for each date was binarized into land and water classes using a threshold value of zero; pixels with values > 0 are land, and those < 0 are water. This process creates a land-water interface. The raster boundary was then converted to a vector polyline using ArcGIS tools, representing the instantaneous shoreline for that date. To minimize the influence of seasonal and daily water level variations, we focus on the dry season (December–March). Additionally, imageries captured during low-tide conditions were used. For recent imagery (Sentinel-2, Landsat 8), acquisition times were cross-referenced with global tidal models (e.g., FES2014) to ensure they represented a low-tide state. However, for historical imagery, where such verification is less reliable, this uncertainty is acknowledged and factored into the calculations (see Section 3.2). This consistent approach to selecting a shoreline proxy ensures maximum comparability throughout the 40-year study period.

3.2. Uncertainty analysis

A Weighted Linear Regression was determined using the total uncertainty value for each shoreline date. This value accounts for various sources of error and is essential for the influence of each shoreline in the regression analysis (Fletcher et al., 2003; Ruggiero et al., 2013). The uncertainty was computed as the square root of the sum of squared errors, using Eq. 2 (Hapke et al., 2011), which is a standard method employed in shoreline change studies worldwide (Boak and Turner, 2005; Thieler et al., 2009).

$$Ut = \sqrt{(Upixel^2 + Ugr^2 + Utide^2)}, \tag{2}$$

where *Upixel* is the pixel resolution error, taken as the spatial resolution of the sensor (e.g., 60 m for MSS, 30 m for TM/ETM+/OLI, 10 m for Sentinel-2). Ugr is the georeferencing error, conservatively estimated as 0.5 pixels for all images. *Utide* is the uncertainty due to tidal variation. This was calculated based on the horizontal shoreline displacement caused by vertical tidal fluctuations. The mean spring tidal range for the region was taken as approximately 1.2 m.

The average beach slope was estimated at 1:30 (a gradient of 0.033), consistent with literature on sandy beaches in the Bight of Benin (Ibe, 1988; Anthony et al., 2015). While local beach morphology will vary along the coast, this regional average represents the best estimation, based on contemporaneous bathymetric surveys for each shoreline date. The potential variation from this average slope is a component of the overall uncertainty. The horizontal uncertainty was therefore calculated as the tidal range divided by the beach slope.

The calculated Ut for each shoreline was entered into the "Uncertainty" attribute field of the shoreline geodatabase, as required by the DSAS tool for the *WLR* analysis. Based on this formula, the calculated total uncertainty (Ut) values, which were input

in the DSAS tool, were approximately ±30.2 m for Landsat MSS images, ±15.1 m for Landsat TM/ETM+/OLI images, and ±5.1 m for the Sentinel-2A image. These values quantitatively informed the weighting in the WLR model, giving higher influence to the more recent, higher-resolution shorelines.

The Landsat imagery data, acquired from 1982 to 2022, was processed using ArcGIS 10.8 for atmospheric correction. A composite band was subsequently created by combining the individual Landsat imagery bands, from which the shorelines were then extracted. To establish the precise location of each shoreline, key attributes including Date, Shape Length, and Uncertainty were added to a geodatabase.

A baseline was defined to cast transects perpendicular to the extracted shorelines and as a reference for calculating distances. It is important to note that this baseline is a computational reference line created for the DSAS analysis and not the official national baseline of Nigeria established under the United Nations Convention on the Law of the Sea (UNCLOS). An official UNCLOS baseline serves legal and jurisdictional purposes, defining the territorial sea and Exclusive Economic Zone.

In contrast, the DSAS baseline's purpose is purely analytical: to be placed parallel to the general trend of the shorelines to ensure that measurement transects are cast orthogonally for accurate change calculation. Using the official UNCLOS baseline, which may be located far offshore or have a different orientation, would not be appropriate for the specific geometric requirements of this geomorphic analysis. A baseline was used for this study, positioned 100 meters offshore and parallel to the 1982 shoreline. The distance between transects was set to 10 m to ensure high-resolution capture of shoreline variability, particularly around the narrow erosional hotspot adjacent to the Badagry Creek inlet. Figure 3 presents shorelines.

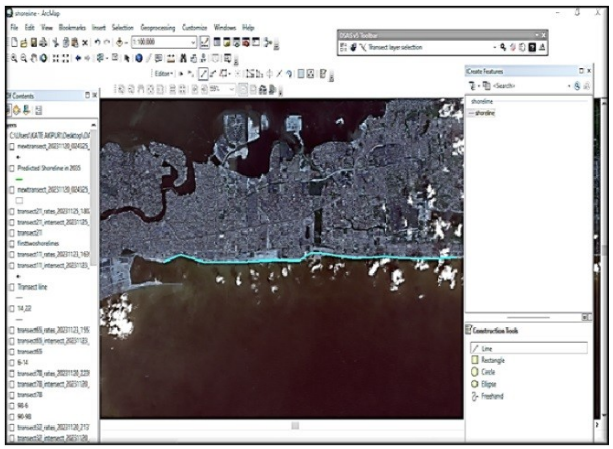

Fig. 3. Extraction of shorelines

Figure 4 illustrates the significant progradation (seaward movement) of the eastern shoreline over the 40 years, alongside the more complex and clustered changes in the central and western sections.

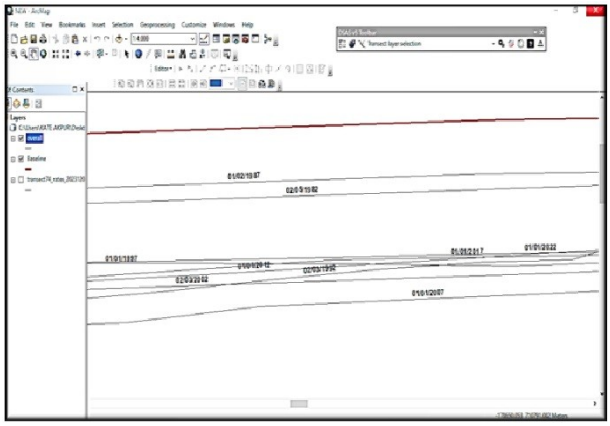

Fig. 4. The multi temporal position of shorelines and baseline (1982-2022)

A shapefile (.shp) was used with the required properties for an offshore baseline 100 m away and nearly parallel to the shoreline. This baseline is to quantify how far the shoreline is from it at each orthogonal transect. The baseline data, received from the DSAS, are shown in Figure 5. It is made concurrently with the casting of the transect. Details such as the polyline shape, casting direction (CastDir), ID, group, and offshore are displayed. The casted transect lines in Figure 5; the baseline is red, and the shorelines are green.

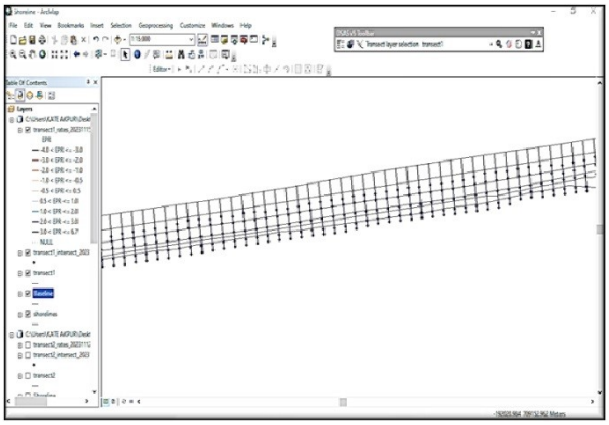

Fig. 5. Casted transect lines

3.3. Shoreline change analysis

The historical change of shorelines was analysed using the Digital Shoreline Analysis System (DSASv5) developed by the United States Geological Survey (Thieler et al., 2009). DSAS computes rate-of-change statistics from multiple historic shoreline positions. The methods used in this study include:

– End Point Rate (*EPR*): Calculated by dividing the distance between the oldest and youngest shorelines (Net Shoreline Movement, NSM) by the time elapsed, shown in Eq. 3 (Thieler et al., 2009).

$$EPR = NSM/(Time\ in\ years). \tag{3}$$

– Linear Regression Rate (*LRR*): This rate is measured by fitting a least-squares regression line to all shoreline positions for a given transect. The *LRR* is the slope of this line, representing the average rate of change over the entire period. It does not have a simple formula like *EPR* because it is a statistical output derived from fitting the model $y = mx + b$ to the data points, where y is the shoreline position, x is time, and m (the *LRR*) is the slope. DSAS calculates this slope for each transect. It is robust because it uses all available data points, making it less susceptible to the influence of outlier shorelines by Dolan et al. (1991).

$$y = mx + b. \tag{4}$$

– Weighted Linear Regression (*WLR*): This is a modified *LRR* designed to incorporate the uncertainty of each shoreline's position. Shorelines with lower uncertainty (e.g., from high-resolution imagery) are given more weight in the regression calculation. The weight (w) is defined as the inverse of the squared uncertainty (e), as established in Eq. 5 (Thieler et al., 2009; Mullick et al., 2019).

$$w = 1/e^2. \tag{5}$$

Beyond calculating rates, DSAS performs a crucial statistical evaluation of the LRR and WLR models for each transect. Two key metrics are used: The R-squared (R^2) value, which assesses the model's goodness of fit by explaining temporal variation in shoreline position, and a 95% Confidence Interval (CI) for each rate. The CI defines the statistical range of the calculated rate, thereby indicating the reliability of the erosion or accretion trend. The future prediction of the shoreline for 2035 was generated using the shoreline forecasting tool in DSAS, which extrapolates from the calculated *LRR* in Eq. 6 (Mullick et al., 2019).

$$Future\ Shoreline\ Position = (LRR \times Time\ Interval) + Intercept \tag{6}$$

4. Results

This section presents the quantitative findings of the shoreline change analysis from 1982 to 2022. The results are organized to first show the temporal variability of shoreline dynamics, followed by an analysis of the long-term spatial patterns of erosion and accretion. The section concludes with a shoreline forecast for the year 2035 based on the calculated long-term rates.

4.1. Temporal variability of shoreline change

The End Point Rate (*EPR*) was quantified using successive 5-year intervals to analyze the short-term dynamics of the coastline. Instead of showing individual maps for each period, Table 2 presents the key statistics. The analysis reveals a highly dynamic system with significant accretion and erosion. Notably, the 2007–2012 period was characterized

by dominant and severe erosion across most of the coastline, with an average rate of –12.07 m/yr. In contrast, other periods, such as 1997–2002 and 2002–2007, were strongly accretionary. The overall 40-year *EPR* (1982–2022) shows a net accretionary trend (average +2.3 m/yr), but with localized erosion reaching –0.65 m/yr (Fig. 6).

Table 2. Summary of End Point Rate (*EPR*) Statistics for Different Time Intervals

Time interval	Average *EPR* (m/yr)	Max accretion (m/yr)	Max erosion (m/yr)	Dominant trend
1982–1987	+3.41	+8.05	–7.50	Accretion
1987–1992	–4.39	+40.97	–8.61	Erosion (with anomalies)
1992–1997	+4.10	+15.26	–16.86	Accretion (with anomalies)
1997–2002	+7.56	+16.99	–4.79	Strong Accretion
2002–2007	+7.47	+14.17	–2.78	Strong Accretion
2007–2012	–12.07	0.00	–19.34	Severe Erosion
2012–2017	+2.26	+7.40	–8.28	Net Accretion
2017–2022	+1.66	+6.00	–8.77	Net Accretion
1982–2022 (overall)	+2.30	+5.52	–0.65	Net Accretion

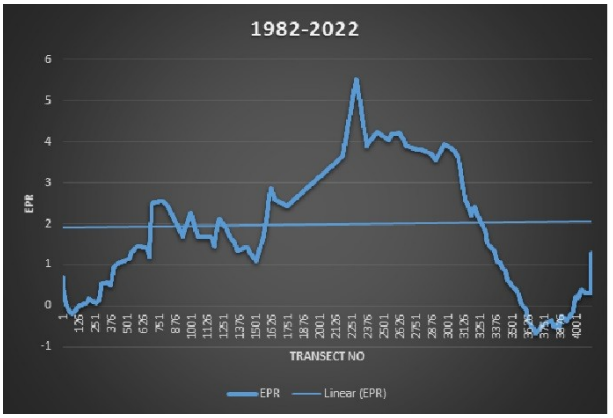

Fig. 6. Shoreline *EPR* from 1982 to 2022

4.2. Long-term spatial patterns of shoreline change

The long-term rates calculated using the Linear Regression Rate (*LRR*) and the Weighted Linear Regression (*WLR*) models offer a more statistically strong perspective of the 40-year trend. The *LRR* model (Fig. 7) demonstrated statistical robustness as an indicator of the long-term trend, directly linking shoreline behavior to persistent drivers.

Across all 4118 transects, the mean value was 0.89, with over 70% of transects yielding a value greater than 0.85, indicating that the linear model explains a very high proportion of the variance in shoreline position over time. The 95% confidence interval for the *LRR* rates (LRR_CI95) further confirmed the certainty of these trends. The model revealed a mean shoreline change rate of +2.42 m/yr. However, the spatial distribution of this change is highly heterogeneous and can be in three distinct zones:

– eastern accretionary zone: The easternmost ~15 km of the coastline is dominated by moderate to high accretion rates, with values ranging from +3.0 to a maximum of +5.32 m/yr.
– central erosional hotspot: A ~10 km segment in the central portion of the study area (spanning approximately from transect ID 1800 to 2800) is a persistent erosion hotspot. Shoreline change rates here are consistently negative, with *LRR* values reaching a maximum erosion rate of –0.28 m/yr.
– western zone of relative stability: The western portion of the coastline exhibits relative stability, with *LRR* change rates generally fluctuating between –1.0 and +1.0 m/yr.

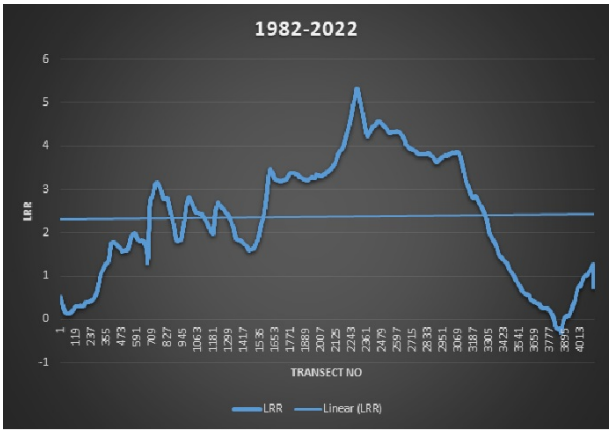

Fig. 7. Shoreline *LRR* from 1982 to 2022

The *WLR* model (Fig. 8), which gives more weight to higher-quality recent data, confirms this spatial pattern, yielding slightly more conservative rates with a maximum accretion of +5.25 m/yr and maximum erosion of –0.21 m/yr.

Figures 6 to 8 show the three zones: stable rates hovering around zero in the west (low transect IDs), a sharp dip into negative values in the central erosional hotspot, and a rise to high positive values in the eastern accretionary zone (high transect IDs). The spatial variability of the long-term trend is most clearly illustrated in Figures 6 to 8, which display the values for each transect along the coast.

It delineates three distinct coastal segments: a western zone of relative stability, a central hotspot of persistent erosion, and an eastern zone of high accretion, quantitatively confirming the patterns observed in the map. Figure 9 compares the predicted 2035

Fig. 8. Shoreline *WLR* from 1982 to 2022

shoreline (green line) with the most recent 2022 shoreline (blue line). The forecast was created by extending the Linear Regression Rate (*LRR*) for each transect, and the comparison visually highlights areas of future erosion and expansion.

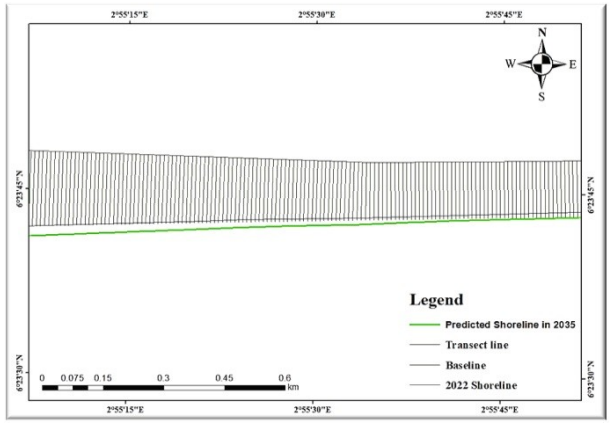

Fig. 9. Forecasted Shoreline Position for 2035

5. Discussion

The results reveal a complex shoreline system where a net accretion trend conceals a critical, localized erosion issue. This discussion interprets the driving forces behind these patterns, compares the findings within a regional context, and outlines the implications for management.

5.1. Interpretation of driving forces: interrupted littoral drift

The spatial patterns of shoreline change along the Badagry coast provide a classic geomorphic signature of an interrupted littoral system. Our analysis reveals a stark dichotomy: persistent, high-rate accretion in the eastern zone (+3.0 to +5.32 m/yr) coexisting with

a concentrated hotspot of chronic erosion in the central zone (–0.28 m/yr, with short-term rates up to –0.65 m/yr). This pattern is not random; it is a direct consequence of the interaction between the natural sediment transport regime and an anthropogenic intervention.

The prominent accumulation of sediment in the east aligns with the well-known net eastward longshore sediment transport in the Bight of Benin (Ibe, 1988; Almar et al., 2015). This area is a natural depositional sink for sediment moving along the coastline. However, a significant finding of this study is that this natural process is affected by artificial means.

The erosion hotspot is situated directly east of the Badagry Creek inlet, confirming that the maintenance of the navigation channel and related structures is the main contributing factor. Our temporal analysis (see Table 2) further supports this, showing that the most severe erosion rate of –12.07 m/yr occurred between 2007 and 2012. This period directly corresponds with reports of a major maintenance dredging campaign at the inlet around 2008, providing a direct temporal link between the anthropogenic activity and the acute shoreline response. These structures act as a sediment trap or a "littoral barrier", sequestering sand that would naturally bypass the inlet to nourish the central coastal segment (Komar, 1998; Mullick et al., 2019).

5.2. Quantitative model assessment and recommendation

A quantitative comparison of the models reveals their distinct strengths and applications for coastal management. The *EPR* captured the most extreme rates (+5.52 m/yr accretion; –0.65 m/yr erosion), highlighting the magnitude of change over short periods but remaining sensitive to outliers (Dolan et al., 1991). In contrast, the *LRR* (+5.32 m/yr accretion; –0.28 m/yr erosion) and *WLR* (+5.25 m/yr accretion; –0.21 m/yr erosion) provided more statistically robust long-term trends.

Factoring in data quality, the Linear Regression Rate (*LRR*) is the preferred method. Its main advantage is that it utilizes all available shoreline data, allowing for a statistically robust trend line less affected by single anomalous events (Fletcher et al., 2003; Ruggiero et al., 2013). The *LRR* in this study demonstrates high R^2 values (averaging 0.89) along with associated confidence intervals, which confirms its reliability. Additionally, the Weighted Linear Regression (*WLR*) offers valuable refinement by considering data quality (Anthony et al., 2015; Mohanty et al., 2015).

The projected shoreline for 2035 was estimated using the robust long-term rate of retreat (*LRR*) in the Digital Shoreline Analysis System (DSAS) forecasting tool. However, the interpretation of this linear forecast is with caution because it assumes stationarity; that is, it presumes that the statistical properties of the system will remain constant (Milly et al., 2008). This assumption faces increasing challenges due to climate change. Linear models fail to account for non-linear accelerations resulting from sea-level rise and changing storm patterns (Ranasinghe, 2016; Vousdoukas et al., 2020). As a result, this forecast reflects a conservative "business-as-usual" scenario rather than a definitive prediction. A comprehensive management strategy should incorporate *LRR* and long-term wave response (*WLR*) for identifying long-term trends, while utilizing extreme event response (*EPR*) to pinpoint periods of significant change that may necessitate immediate tactical responses.

However, a quantitative comparison of the models reveals their distinct strengths and applications for coastal management. The End Point Rate (*EPR*) captured the most extreme short-term changes, with a maximum accretion of +5.52 m/yr and erosion of –0.65 m/yr, making it possible to identify periods of acute change linked to specific events like major storms or dredging campaigns. In contrast, the Linear Regression Rate (*LRR*) is the recommended method. Providing a more moderate trend (max accretion +5.32 m/yr; max erosion –0.28 m/yr), the *LRR* utilizes all available shoreline data, resulting in a statistically robust trend line less influenced by single anomalous events (Dolan et al., 1991). The high mean R^2 values of 0.89 in this study confirm its reliability. The Weighted Linear Regression (*WLR*), which gave the most conservative estimates (max accretion +5.25 m/yr; max erosion –0.21 m/yr), is also highly valuable as it refines the *LRR* by considering data quality (Mullickz et al., 2019).

6. Conclusion

This study successfully quantified forty years of shoreline dynamics along the Badagry coast, revealing a deceptive narrative of overall accretion that conceals a critical, anthropogenically driven erosion hotspot. By integrating multi-sensor satellite imagery from 1982 to 2022 within the DSAS framework, we demonstrated that human activities at the Badagry Creek inlet have interrupted the regional longshore transport system, causing chronic downdrift erosion, a classic pattern of an interrupted littoral system documented in diverse coastal settings worldwide. The Linear Regression Rate model, validated by high statistical confidence (> 0.9), proved most robust for identifying this long-term, spatially-defined problem.

The main conclusion of this research is that a uniform coastal management policy for Badagry is ineffective and potentially wasteful. Instead, allocate resources to a targeted strategy that addresses sediment starvation at the specific erosion hotspot. It could involve engineered sediment bypassing or an ongoing beach nourishment programme.

While this study robustly establishes historical trends, we acknowledge that the linear forecasting models have limitations. They assume that the rates and causes of past change will continue unchanged. This approach cannot account for non-linear accelerations associated with climate change, such as accelerated sea-level rise and increased storm intensity or frequency, which worsen coastal erosion globally (Vousdoukas et al., 2020; IPCC, 2023). Future research must therefore pivot towards process-based numerical models (e.g., Delft3D, XBeach) to project shoreline positions under various climate scenarios (Lyddon et al., 2021). Such models could simulate sediment transport pathways and test the efficacy of potential interventions, such as a sediment bypassing system or optimized beach nourishment designs. Integrating the outputs of these physical models with socio-economic vulnerability assessments will be crucial for developing a truly resilient and sustainable management plan for the Badagry coastline.

Author contributions

Conceptualization E.A.; methodology: E.A., K.A.; writing the original draft: E.A.; formal analysis and investigation: E.A., K.A.; validation: E.A., O.G., J.O.; writing-review, and editing: E.A., O.G., J.O.; supervisor: E.A.

Data availability statement

The data that support the findings of this study are available from the corresponding author upon reasonable request.

Acknowledgements

The authors would like to thank the anonymous reviewers and the editor for their constructive comments and contributions.

References

Adeaga, O., Folorunsho, R., Foli, B.A.K. et al. (2021). Assessment of Shoreline Change Along the Coast of Lagos, Nigeria. *Remote Sens. Earth Sys. Sci.*, 4, 186–198. DOI: 10.1007/s41976-021-00059-w.

Adesina, E.A., Musa, A., Ajayi, O.G. et al. (2022). Comparative assessment of SRTM and UAV-Derived DEM in flood modelling. *Environ. Tech. Sci. J.*, 12(2), 58–70. DOI: 10.4314/etsj.v12i2.6.

Ajayi, O.G., Kolade, T.S., and Baba, M. (2023). *Mapping and assessing the seasonal dynamics of surface urban heat intensity using LandSAT-8 OLI/TIRS images*. In Climate Change Impacts on Nigeria: Environment and Sustainable Development (pp. 261–277). Cham: Springer International Publishing.

Almar, R., Kestenare, E., Reyns, J. et al. (2015). Response of the Bight of Benin (Gulf of Guinea, West Africa) coastline to anthropogenic and natural forcing, Part1: Wave climate variability and impacts on the longshore sediment transport. *Continental Shelf Research*, 110(1), 48–59. DOI: 10.1016/j.csr.2015.09.020.

Aman, A., Tano, R.A., Toualy, E. et al. (2019). Physical forcing induced coastal vulnerability along the Gulf of Guinea. *J. Environ. Prot.*, 10, 1194–1211. DOI: 10.4236/jep.2019.109071.

Anthony, E.J., Almar, R., and Aagaard, T. (2015). *The Bight of Benin, a major transgressive deltaic shoreline: morphodynamic settings and shoreline mobility*. In E.J. Anthony (Ed.), Geomorphology of the world's river deltas (pp. 1–13).

Anthony, E.J., Brunier, G., Besset, M. et al. (2019). Linking rapid erosion of the Mekong River delta to human activities. *Sci. Rep.*, 9(1), 1–12. DOI: 10.1038/srep14745.

Arjasakusuma, S., Kusuma, S.S., Saringatin, S. et al. (2021). Shoreline dynamics in East Java Province, Indonesia, from 2000 to 2019 using multi-sensor remote sensing data. *Land*, 10(2), 100. DOI: 10.3390/land10020100.

Boak, E.H., and Turner, I.L. (2005). Shoreline definition and detection: A review. *J. Coastal Res.*, 21(1), 688–703. DOI: 10.2112/03-0071.1.

Boateng, I., Wiafe, G., and Jayson-Quashigah, P.N. (2016). Mapping Vulnerability and Risk of Ghana's Coastline to Sea Level Rise. *Marine Geodesy*, 40(1), 1-24. DOI: 10.1080/01490419.2016.1261745.

Brown, S., Nicholls, R.J., Lowe, J.A. et al. (2017). Spatial variations of sea-level rise and impacts: An application of DIVA. *Clim. Change*, 134, 403–416. DOI: 10.1007/s10584-013-0925-y.

Cooper, J.A., Masselink, G., Coco, G. et al. (2020). Sandy beaches can survive sea-level rise. *Nature Clim. Change,* 10(11), 993–995. DOI: 10.1038/s41558-020-00934-2.

Daniela, P.D., D'Alessandro, F., Riefolo, L. et al. (2018). Application of a Coastal Vulnerability Index. A Case Study along the Apulian Coastline, Italy. *Water*, 10(9), 1218. DOI: 10.3390/w10091218.

Dolan, R., Fenster, M.S., and Holme, S.J. (1991). Temporal analysis of shoreline recession and accretion. *J. Coastal Res.*, 731–744.

Donchyts, G., Baart, F., Winsemius, H. et al. (2016). Earth's surface water changes over the past 30 years. *Nature Clim. Change,* 6(9), 810–813. DOI: 10.1038/nclimate3111.

Duru, U. (2017). Shoreline change assessment using multi-temporal satellite images: a case study of Lake Sapanca, NW Turkey. *Environ. Monitoring Assess.*, 189, 385. DOI: 10.1007/s10661-017-6112-2.

Fletcher, C.H., Rooney, J., Barbee, M. et al. (2003). Mapping shoreline change using digital orthophotogrammetry on Maui, Hawaii. *J. Coastal Res.*, 38(SI), 106–124.

Giardino, A., den Heijer, C., and Deltares. (2018). Global distribution of coastal risk. *JRC Tech. Repo., EUR 29428 EN*.

Gumus, M.G., Durduran, S.S., and Gümüs, K. (2021). Investigation of shoreline change rates using the digital shoreline analysis system in Lake Beyşehir, Turkey. *Bull. Geophys. Oceanogr.*, 63(1), 119–142. DOI: 10.4430/bgo00369.

Hakkou, M., Maanan, M., Bendaoud, B. et al. (2018). Multi-decadal analysis of shoreline changes using geospatial tools and automatic computation in Kenitra coast, Morocco. *Ocean Coastal Management*, 163, 232–239. DOI: 10.1016/j.ocecoaman.2018.07.003.

Hapke, C.J., Himmelstoss, E.A., Kratzmann, M.G. et al. (2011). *National assessment of shoreline change: Historical shoreline change along the New England and Mid-Atlantic coasts*. U.S. Geological Survey Open-File Report 2010–1118.

Ibe, A.C. (1988). *Coastline erosion in Nigeria*. Ibadan University Press.

IPCC. (2023). *Synthesis Report of the IPCC Sixth Assessment Report (AR6)*. Intergovernmental Panel on Climate Change.

Jawak, S.D., and Luis, A.J. (2014). A semiautomatic extraction of Antarctic lake features using WorldView-2 imagery. *Photogr. Eng. Remote Sens.*, 80(10), 939–952. DOI: 10.14358/PERS.80.10.939.

Komar, P.D. (1998). Tidal-Inlet Processes and Morphology Related to the Transport of Sediments. *J. Coastal Res.*, 26, 23–45.

Komolafe, A.A., Apalara, P.A., Ibitoye, M.O. et al. (2022). Spatio-temporal Analysis of Shoreline Positional Change of Ondo State Coastline Using Remote Sensing and GIS: A Case Study of Ilaje Coastline at Ondo State in Nigeria. *Earth Sys. Environ.*, 6, 281–293. DOI: 10.1007/s41748-021-00270-1.

Luijendijk, A., Hagenaars, G., Ranasinghe, R. et al. (2018). The state of the world's beaches. *Sci. Rep.*, 8(1), 1–11. DOI: 10.1038/s41598-018-24630-6.

Lyddon, C.E., Bird, C., Brown, J.M. et al. (2021). *Application of x-band radars for deriving intertidal bathymetries and characterising coastal behaviours (National Oceanography Centre Internal Document, No. 23)*. National Oceanography Centre.

McDonnell, T. (2019). The refugees the world barely pays attenti on to. *NPR Goats and Soda*.

Mentaschi, L., Vousdoukas, M.I., Pekel, J.F. et al. (2018). Global long-term analysis of coastal erosion and accretion. *Sci. Rep.*, 8(1), 1–12. DOI: 10.1038/s41598-018-30904-w.

Milly, P.C.D., Betancourt, J., Falkenmark, M. et al. (2008). Stationarity is dead: Whither water management? *Science*, 319(5863), 573–574. DOI: 10.1126/science.1151915.

Mobio, B., Doumbia, S., Tiemele, J. et al. (2024). *Coastal Vulnerability Assessment of the Tabou-Fresco Coastline (Côte D'Ivoire) Using Earth Observation Data.* In J. Potel, K. Labbassi, S. Tesfamichael, H. Annegarn, J. Kufoniyi, and S. Wade (Eds.), Space and Geospatial Technologies for the Africa We Want. Southern Space Studies: Springer. DOI: 10.1007/978-3-031-64213-5_21.

Mohanty, P.K., Barik, S.K., Kar, P.K. et al. (2015). Impacts of Ports on Shoreline Change Along Odisha Coast. *Procedia Eng.*, 116, 647–654. DOI: 10.1016/j.proeng.2015.08.339.

Mullick, M.R., Tanim, A., and Samiul, I.S.M. (2019). Coastal vulnerability analysis of Bangladesh coast using fuzzy logic based geospatial techniques. Ocean Coastal Manage., 174, 154-169. DOI: 10.1016/j.ocecoaman.2019.03.010.

Natesan, U., Thulasiraman, N., Deepthi, K. et al. (2013). Shoreline change analysis of Vedaranyam coast, Tamil Nadu, India. *Environ. Monitoring Assess.*, 185, 5099—5109. DOI: 10.1007/s10661-012-2928-y.

Neide, P.A., Pedro, J.M.C., and Alexandre, O.T. (2022). Social engagement in coastal adaptation processes: Development and validation of the Coast ADAPT scale. *Environ. Sci. Policy*, 133, 107–114. DOI: 10.1016/j.envsci.2022.03.011.

Nicholls, R.J., Marinova, N., Lowe, J.A. et al. (2011). Sea-level rise and its possible impacts given a 'beyond 4 C world' in the twenty-first century. *Philosophical Trans. Royal Soc.Math., Physical Eng. Sci.*, 369(1934), 161–181. DOI: 10.1098/rsta.2010.0291.

Obowu, C.D., and Abam, T.K. (2014). Spatial and multi-temporal change analysis of the Niger Delta coastline using remote sensing and geographic information system (GIS). *Int. J. Remote Sens. App.*, 4(1), 41–49.

Ogunrayi, O.A., Mattah, P.A.D., Folorunsho, R. et al. (2023). A Spatio-Temporal Analysis of Shoreline Changes in the Ilaje Coastal Area of Ondo State, Nigeria. *J. Marine Sci. Eng.*, 2(1), 18. DOI: 10.3390/jmse12010018.

Oyedepo, J., and Oluyege, D. (2024). Spatiotemporal assessment of wetlands and land reclaim activities in Eastern Lagos State Nigeria. *Nigerian J. Tech.*, 43(3), 577–586. DOI: 10.4314/njt.v43i3.21.

Pollard, D., DeConto, R.M., and Alley, R.B. (2015). Potential Antarctic Ice Sheet retreat driven by hydrofracturing and ice cliff failure. *Earth Planet. Sci. Lett.*, 412, 112–121. DOI: 10.1016/j.epsl.2014.12.035.

Ranasinghe, R. (2016). Assessing climate change impacts on sandy coasts: A review. *Earth-Sci. Rev.*, 160, 320–332. DOI: 10.1016/j.earscirev.2016.07.011.

Roy, S., Mahapatra, M., and Chakraborty, A. (2018). Shoreline change detection along the coast of Odisha, India using digital shoreline analysis system. *Spatial Inf. Res.*, 26, 563–571. DOI: 10.1007/s41324-018-0199-6.

Ruggiero, P., Kaminsky, G.M., Gelfenbaum, G. et al. (2013). *National assessment of shoreline change: Historical shoreline change along the Pacific Northwest coast*. U.S. Geological Survey Open-File Report, 2012–1007.

Shetty, A., Jayappa, K.S., and Mitra, D. (2015). Shoreline Change Analysis of Mangalore Coast and Morphometric Analysis of Netravathi-Gurupur and Mulky-pavanje Spits. *Aquatic Procedia*, 4, 182–189. DOI: 10.1016/j.aqpro.2015.02.025.

Smail, E.A., DiGiacomo, P.M., Seeyave, S. et al. (2019). An introduction to the 'Oceans and Society: Blue Planet' initiative. *J. Operational Oceanogr.*, 12(sup2), S1–S11. DOI: 10.1080/1755876X.2019.1634959.

Tiemele, J., Agoua, A., and Brice Mobio, B. (2022). Mapping of Coastal Hazards in the South-West of Côte d'Ivoire on SRTM Images. *Adv. Remote Sens.*, 11(3), 158–166.

Thakur, S., Dey, D., Das, P. et al. (2017). Shoreline change detection using remote sensing in the Bakkhali coastal region, West Bengal, India. *Indian J. Geosci.*, 71(4), 611–626.

Thieler, E.R., Himmelstoss, E.A., Zichichi, J.L. et al. (2009). *Digital Shoreline Analysis System (DSAS) version 4.0 – An ArcGIS extension for calculating shoreline change*. US Geological Survey Open-File Report, 2008–1278.

Vousdoukas, M.I., Ranasinghe, R., Mentaschi, L. et al. (2020). Sandy coastlines under threat of erosion. *Nature Clim. Change,* 10(1), 364–367. DOI: 10.1038/s41558-020-0697-0.

WACOM. (2023). *West Africa Coastal Observatory Mission*.

Wang, X., Liu, Y., Ling, F. et al. (2017). Spatio-temporal change detection of Ningbo coastline using Landsat time-series images during 1976—2015. *ISPRS Intl. J. Geo-Inf.*, 6(3), 68. DOI: 10.3390/ijgi6030068.

Wu, Q., Miao, S., Huang, H. et al. (2022). Quantitative analysis on coastline changes of Yangtze River Delta based on high spatial resolution remote sensing images. Remote Sens., 14(2), 310. DOI: 10.3390/rs14020310.

Xu, H. (2006). Modification of normalised difference water index (NDWI) to enhance open water features in remotely sensed imagery. *Int. J. Remote Sens.*, 27(14), 3025–3033. DOI: 10.1080/01431160600589179.

Young, A.P., and Carilli, J.E. (2018). Global distribution of coastal cliffs. *Earth Surface Proces and Landforms*, 44(6), 1309–1316. DOI: 10.1002/esp.4574.

Zhou, X., Wang, J., Zheng, F. et al. (2023). An Overview of Coastline Extraction from Remote Sensing *Data. Remote Sens.*, 15(19), 4865. DOI: 10.3390/rs15194865.